Breaking tolerance with engineered class I antigen-presenting molecules

Christopher A. Parks[a,b], Kalli R. Henning[a], Kevin D. Pavelko[a], Michael J. Hansen[a], Virginia P. Van Keulen[a], Brendan K. Reed[a,b], Jennifer D. Stone[c], Adam G. Schrum[d,e,f], Diana Gil[d,e,f], David M. Kranz[g], Andrew J. Bordner[h], Michael A. Barry[i], and Larry R. Pease[a,1]

[a]Department of Immunology, Mayo Clinic, Rochester, MN 55905; [b]Immunology PhD Program, Mayo Clinic Graduate School of Biomedical Sciences, Rochester, MN 55905; [c]AbbVie Inc., North Chicago, IL 60064; [d]Department of Molecular Microbiology and Immunology, University of Missouri School of Medicine, Columbia, MO 65212; [e]Department of Surgery, University of Missouri School of Medicine, Columbia, MO 65212; [f]Department of Bioengineering, University of Missouri, Columbia, MO 65212; [g]Department of Biochemistry, University of Illinois, Urbana, IL 61801; [h]Sutter Health Design and Innovation, San Carlos, CA 94070; and [i]Department of Internal Medicine, Division of Infectious Diseases, Mayo Clinic, Rochester, MN 55905

Edited by Hidde L. Ploegh, Boston Children's Hospital, Boston, MA, and approved January 8, 2019 (received for review April 30, 2018)

Successful efforts to activate T cells capable of recognizing weak cancer-associated self-antigens have employed altered peptide antigens to activate T cell responses capable of cross-reacting on native tumor-associated self. A limitation of this approach is the requirement for detailed knowledge about the altered self-peptide ligands used in these vaccines. In the current study we considered allorecognition as an approach for activating CTL capable of recognizing weak or self-antigens in the context of self-MHC. Nonself antigen-presenting molecules typically contain polymorphisms that influence interactions with the bound peptide and TCR interface. Recognition of these nonself structures results in peptide-dependent alloimmunity. Alloreactive T cells target their inducing alloantigens as well as third-party alloantigens but generally fail to target self-antigens. Certain residues located on the alpha-1/2 domains of class I antigen-presenting molecules primarily interface with TCR. These residues are more conserved within and across species than are residues that determine peptide antigen binding properties. Class I variants designed with amino acid substitutions at key positions within the conserved helical structures are shown to provide strong activating signals to alloreactive CD8 T cells while avoiding changes in naturally bound peptide ligands. Importantly, CTL activated in this manner can break self-tolerance by reacting to self-peptides presented by native MHC. The ability to activate self-tolerant T cells capable of cross-reacting on self-peptide-MHC in vivo represents an approach for inducing autoimmunity, with possible application in cancer vaccines.

cancer immunotherapy | MHC | T cells | tolerance | adenovirus

T cells are capable of mounting responses against cancer through recognition of tumor-associated antigens (1–4). Neoantigens and overexpressed antigens are currently the primary focus for immunotherapy; however, their occurrence is relatively rare with most potential antigens presented by the tumor being unaltered self-peptides (4–6). Furthermore, due to heterogeneity in tumor cellularity, the most prevalent antigens shared by all tumor cells are these unaltered tumor-associated self-peptides (7, 8). The available peripheral T cell repertoire is selected against receptors bearing high affinity for self-ligands (9–12), thus limiting the capacity of the immune system to attack and destroy tumors. The residual weak recognition of self-ligands in the periphery transduces subthreshold signals through the T cell antigen receptor (TCR) that maintains TCR sensitivity and immune homeostasis but by itself is incapable of providing full activation (13–15). In this way, central tolerance has limited the available T cell repertoire capable of responding to cancer with high affinity (16–18) but maintains a focus of the immune repertoire on self (19).

Self-tolerant T cells can become autoreactive once activated (20, 21). Efforts to exploit these T cells employ approaches to enhance their activation using alternative ligands or by lowering the activation threshold (22, 23). Cancers with higher mutational rates produce cancer-specific peptides that potentially result in neoantigens capable of driving T cell immunity (24). However, because most of these immunogenic mutations occur during cancer progression, only a subset of clones making up the tumors are expected to express these antigens (25). Furthermore, mechanisms of peripheral tolerance and properties intrinsic to cancers contribute to curbing potential T cell responses against these newly formed tumor antigens (26). Therefore, although recognition of neoantigens is sufficient to activate T cells against cancer, it is generally insufficient to provide durable and curative antitumor responses (27).

Methods to break tolerance would be useful in cancer immunity. Current approaches include developing vaccines to activate low-affinity T cells (22, 28), therapeutic interventions such as checkpoint inhibitors to disrupt mechanisms of peripheral tolerance (29), and introduction of surrogate high-affinity T cell receptors into T cells to target cancer-associated antigens (30). None of these approaches are sufficiently developed to meet all of the needs of cancer patients. Here we describe a vaccination

Significance

Provision of sufficient activating signals can drive self-tolerant T cells to cross-react on self-peptide-MHC in a breakdown of tolerance. This approach has been applied in the development of heteroclitic peptide vaccines, which retain sufficient similarity to self to allow reactivation of effector cells on unaltered self-epitopes but require detailed knowledge about the behavior of individual altered self-peptide antigens. We designed altered-self MHC mutant antigen-presenting molecules to drive CTL capable of cross-reacting on self-peptide-MHC and demonstrate the breaking of self-tolerance to defined and undefined self-antigens. These findings bear particular importance in the field of cancer immunotherapy in which breaking tolerance to weakly antigenic cancer-associated antigens is fundamental to vaccination strategies.

Author contributions: C.A.P., K.D.P., V.P.V.K., B.K.R., A.G.S., D.G., A.J.B., M.A.B., and L.R.P. designed research; C.A.P., K.R.H., M.J.H., V.P.V.K., B.K.R., and A.J.B. performed research; J.D.S., A.G.S., D.G., D.M.K., A.J.B., and M.A.B. contributed new reagents/analytic tools; C.A.P., V.P.V.K., B.K.R., A.J.B., and L.R.P. analyzed data; and C.A.P. and L.R.P. wrote the paper.

Conflict of interest statement: The authors have a pending US patent application, US20160361402A1, relevant to the delivery of MHC class I heavy chain mutant genes using adenoviral transduction in humans.

This article is a PNAS Direct Submission.

[1]To whom correspondence should be addressed. Email: pease.larry@mayo.edu.

This article contains supporting information online at www.pnas.org/lookup/suppl/doi:10.1073/pnas.1807465116/-/DCSupplemental.

Published online February 6, 2019.

platform designed to break tolerance to weakly antigenic peptides. Our approach couples strong stimulation of self-reactive T cells with the biological selection of residual elements of the T cell repertoire capable of recognizing a spectrum of undefined self-antigens.

This platform was developed using molecular mechanics modeling to predict mutant MHC antigen-presenting molecules with enhanced binding stability for self-reactive T cell receptors. The mutant molecules are expressed in lymph node (LN) resident APCs to drive autoreactive immune responses in vivo. The evidence presented demonstrates that a vaccine based on this approach can break tolerance.

Results

Single Amino Acid Substitutions of H-2K^b Heavy Chain Designed to Enhance TCR Binding but Not Peptide Binding. A combination of structural analysis and molecular mechanics (MM) modeling was performed to model the consequence of amino acid substitutions in MHC class I molecules. The analysis identified amino acid substitutions predicted to enhance the stability of TCR–pMHC interactions while preserving normal peptide presentation. The overall goal of this process was to design class I molecules that could activate alloreactive T cell responses capable of cross-reacting with self-pMHC. Candidate residues were chosen for modeling based on known interactions with TCR as reported from structural analyses in the literature (31–33) and prediction of the TCR–pMHC interface using PDBePISA (34). These residues are shown in *SI Appendix*, Fig. S1*A*, and with TCR CDR loops overlaid in *SI Appendix*, Fig. S1*B*. MM was used to predict changes in binding energy of the sum of TCR–pMHC interactions after systematically replacing each residue shown in *SI Appendix*, Fig. S1*A*, with all other possible amino acids. We considered the prototypic TCR–pMHC ternary bound structures available when the analysis was initiated in 2012. Modeling was performed using two sets of related TCR–pMHCI structures complexed with different peptides, one set human and one set mouse. The analyzed structures were HLA-A*02:01 with wild-type Tax peptide (35) (Fig. 1*A*), Tax variant peptide V7R (36) (Fig. 1*B*), and haptenated Tax variant peptide Tax5K-IBA (37) (Fig. 1*C*) each in complex with the A6 TCR; H-2K^b with dEV-8 peptide (31) (Fig. 1*D*) and SIY peptide (Fig. 1*E*) (31) both in complex with the 2C TCR. As shown in Fig. 1, amino acid substitutions that enhanced stability (−ΔΔG) are shown in blue, whereas substitutions that decreased stability (+ΔΔG) are shown in red. Considering only residues modeled in both human and mouse structures, out of 323 possible mutants, 32 were identified that consistently enhanced TCR–pMHC stability across all five structures modeled. Of these 32 mutants, 4 were identified that primarily interact with the germline encoded CDR2α/β loops of the TCR and do not interact with the bound peptide ligand. Remarkably, the analysis predicted tryptophan (W) substitution at each of these positions as stabilizing. Fig. 2 shows the four mutants identified: Q72W (Fig. 2*A*), V76W (Fig. 2*B*), A158W (Fig. 2*C*), and G162W (Fig. 2*D*). To study whether these four MHC class I mutants behaved as predicted, each of the four residues were mutated individually in the H-2K^b gene. Mouse L cells were stably transfected with genes encoding the H-2K^b heavy chain mutated to W individually at each of the four predicted positions. L cells were also stably transfected with wild-type H-2K^b or with H-2L^d to serve as controls. L cell transfectants were cloned by limiting dilution. To determine if introducing W substitutions at the solvent exposed TCR interface of H-2K^b altered expression of the molecule, a panel of conformation-dependent anti–H-2K^b mAbs was used. Surface expression of each mutant was confirmed by flow cytometry using multiple K^b-specific mAbs, indicating that the single amino acid substitutions did not perturb the ability of the mutant molecules to fold and be expressed at the cell surface in comparison with WT K^b (*SI Appendix*, Fig. S2).

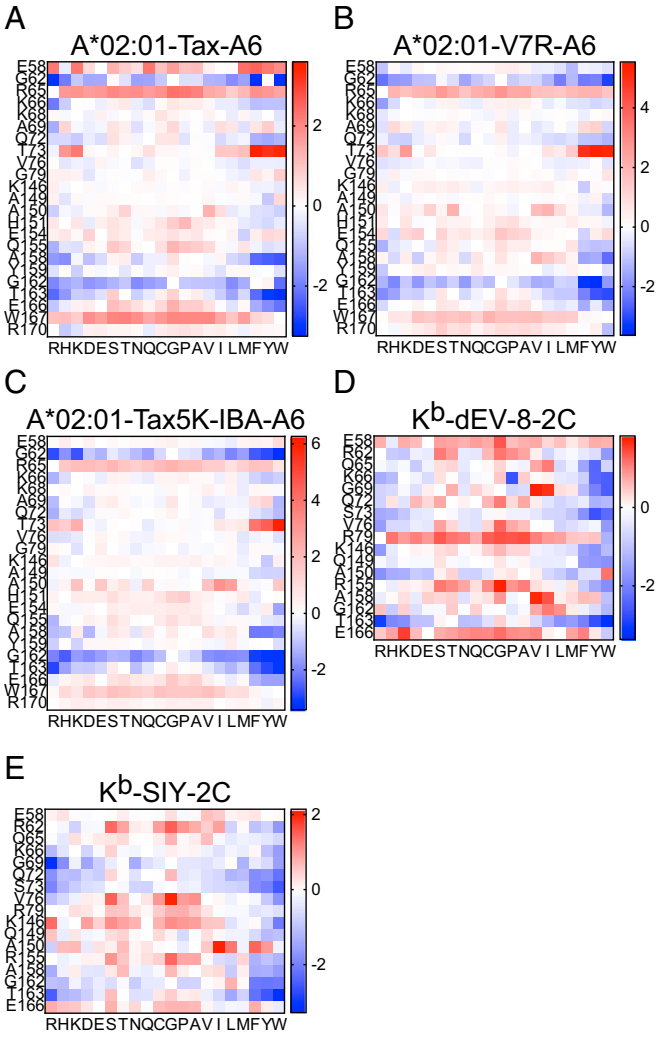

Fig. 1. MM modeling of TCR-pMHC to estimate binding energy following amino acid replacements on the class I heavy chain at the TCR interface. (*A*–*E*) Heat maps represent increases (red) or decreases (blue) in predicted Gibb's free energy. Positions of evaluated amino acids of MHC class I heavy chain are indicated on the *y* axes for each receptor ligand pair. Substituted amino acid is indicated on the *x* axes for the modeled structures: (*A*) A6 TCR in complex with HLA-A*02:01 and wild-type Tax peptide, (*B*) A6 TCR in complex with HLA-A*02:01 and Tax peptide variant V7R, (*C*) A6 TCR in complex with HLA-A*02:01 and haptenated Tax variant peptide Tax5K-IBA, (*D*) 2C TCR in complex with H-2K^b and dEV-8 peptide, and (*E*) 2C TCR in complex with H-2K^b and SIY peptide.

K^b Mutants Q72W and G162W Do Not Fundamentally Alter Peptide Presentation. Two variants, Q72W and G162W, were selected in an analysis of peptide binding. Because the residue positions of the predicted K^b mutants appear to primarily facilitate interaction with TCR CDR2 loops and do not interact with bound peptide ligand (*SI Appendix*, Fig. S1*B*), we hypothesized that peptide binding would not be affected by amino acid substitution at these sites. We tested the hypothesis by quantifying peptide binding using competitive inhibition (Fig. 3). L cell transfectants were pulsed with biotinylated reference peptide, SII[C-biotin] FEKL (38), and varying concentrations of nonlabeled competitor peptides before staining with streptavidin-PE. Measurement of reference peptide binding was determined using flow cytometry.

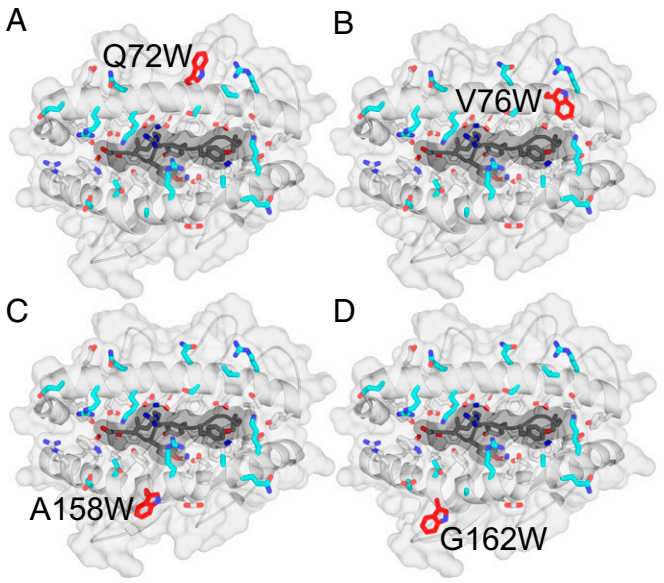

Fig. 2. The H-2K^b class I heavy chain mutated to tryptophan at four key positions determined by MM modeling. Positions chosen for amino acid substitution based on MM modeling and structural analysis are (*A*) Q72W, (*B*) V76W, (*C*) A158W, and (*D*) G162W. Mutation to W at each of the four positions was predicted to be stabilizing in the context of the ternary structures on which they were modeled.

Nonlinear regression was used to generate binding curves of reference peptide binding for each of the MHC molecules tested—K^b, Q72W, and G162W—when competed with varying concentrations of competitor peptides OVA (Fig. 3*A*), TRP2 (Fig. 3*B*), and VSV (Fig. 3*C*). Comparison of binding curves using a test of best fit between K^b and K^b mutants Q72W and G162W revealed no significant differences in reference peptide binding. Because most of our subsequent in vivo antigen-presenting studies used the amino acid 72 and 162 variants, fine mapping of peptide binding by the mutants V76W and A158W was not evaluated.

Binding of the m67 Single-Chain to the K^b Mutant:SIY Ligand Complexes. The tryptophan class I mutants were predicted to enhance stability of TCR–pMHC interaction in the five crystal structures modeled. To evaluate this prediction, we measured TCR binding for K^b and K^b mutants using a biotinylated soluble single-chain TCR (scTCR) developed as a high-affinity variant of 2C with specificity for the peptide antigen SIY (39–41). Human TAP-deficient T2 transfectants stably expressing K^b or K^b mutants Q72W, V76W, A158W, and G162W were loaded with either the cognate peptide SIY or negative control peptide OVA. Cell surface levels of each peptide loaded class I molecule were measured using the alpha-3 D^d epitope recognized by the 34-2-12 antibody. After peptide loading, T2-K^b and T2-K^b mutant transfectants were pulsed with biotinylated scTCR followed by streptavidin-BV421, and the measured binding was normalized to total class I expression. Binding of scTCR to each of the T2 cell lines loaded with SIY and negative control OVA peptides was assessed (*SI Appendix*, Fig. S3*A*, *Top*), as were the total levels of K^b and K^b mutant expression after peptide loading (*SI Appendix*, Fig. S3*A*, *Bottom*). Binding of scTCR for T2-K^b mutants Q72W, V76W, and A158W was significantly decreased compared with binding for T2-K^b, indicating that in the context of this specific interaction these mutations interfere with binding for the TCR single-chain probe (*SI Appendix*, Fig. S3*A*, *Top* and second, third, and fourth panels, and *SI Appendix*, Fig. S3*B*). However, binding of scTCR to the T2- K^b mutant G162W was significantly increased compared with binding for T2-K^b under these conditions (*SI Appendix*, Fig. S3*A*, *Top* and *Right*, and *SI Appendix*, Fig. S3*B*). To evaluate whether the introduction of W at residue 162 improved binding to the scTCR, a titration was performed, revealing a similar EC_{50} for both the G162W and WT K^b ligands (*SI Appendix*, Fig. S3*C*). However, at high concentrations, enhanced binding to K^{b}G162W:SIY was observed, even in the absence of increased class I expression on the cell surface (*SI Appendix*, Fig. S3*C*). This raised the possibility that more K^{b}G162W molecules were loaded with peptide antigen than were K^b molecules in the comparison. Using a competitive inhibition of peptide binding assay, we evaluated the possibility that the increased binding of scTCR to the K^{b}G162W mutant at high concentrations was due to increased SIY binding to the mutant MHC molecule. Consistent with our conclusion that the mutation does not influence peptide binding (as summarized in Fig. 3), we found essentially identical binding to the parental and mutant MHC molecules ($-\text{LogIC}_{50}$ 7.734 M vs. 7.726 M, P = 0.9715). Although these findings indicate greater binding of the scTCR to the K^b mutant G162W at higher receptor/ligand concentrations, we cannot attribute this simply to the predicted enhanced stability of the MHC:peptide ligand for the scTCR. Nonetheless, the introduction of W substitutions at the interface between the MHC:peptide complex and TCR appears to alter receptor/ligand interactions.

Recognition of K^b Mutants by an H-2^b–Restricted T Cell Repertoire Results in Expansion and Cytotoxic Differentiation of CD8 T Cells in Vitro. We next assessed the functional ability of the predicted K^b mutants to be recognized by CD8 T cells. We hypothesized that if the predicted K^b mutants could act as functional antigen-presenting molecules, then recognition of the K^b mutants by CD8 T cells from K^b-tolerant mice would result in T cell activation. We tested this hypothesis by culturing CFSE-labeled CD8 T cells from B6C3F1 mice with L cell transfectants stably expressing WT K^b or the K^b mutants Q72W, V76W, A158W, and G162W. Because L cells are derived from C3H mice, B6C3F1 mice were used for their tolerance to H-2^b and H-2^k alleles, along with C3H-encoded minor peptide antigens. Fig. 4 *A*–*D* shows the proliferation and differentiation of B6C3F1 CD8

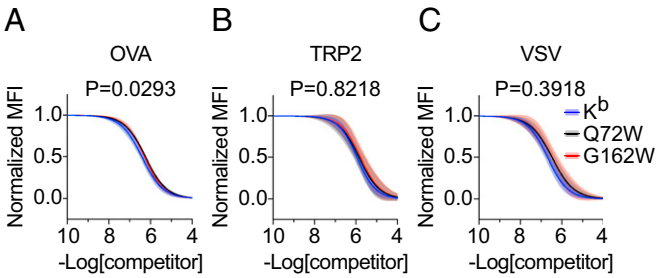

Fig. 3. K^b mutants Q72W and G162W display unaltered peptide binding properties. (*A*–*C*) Stable L cell transfectants expressing K^b or K^b mutants Q72W and G162W were loaded with a biotinylated reference peptide SII[C-biotin]FEKL and increasing concentrations of unlabeled competitor peptides $OVA_{257–264}$ (*A*), $TRP2_{180–188}$ (*B*), and $VSV_{52–59}$ (*C*). After peptide loading and staining with streptavidin-PE, flow cytometry was used to quantify reference peptide binding for each titration of competitor. Variable-slope, nonlinear regression was used to fit inhibition curves (solid lines), normalized by the maximum and minimum values, using two independent measurements at each competitor peptide concentration. Error bands represent the 95% confidence intervals (shaded) of the inhibition curves. $R^2 > 0.94$ for all inhibition curves. The extra sum-of-squares F test was used to assess statistically significant differences among inhibition curves. The null hypothesis that K^b, Q72W, and G162W bound each competitor peptide equivalently was not rejected based on the multiple comparisons corrected significance threshold of $P < 0.0167$.

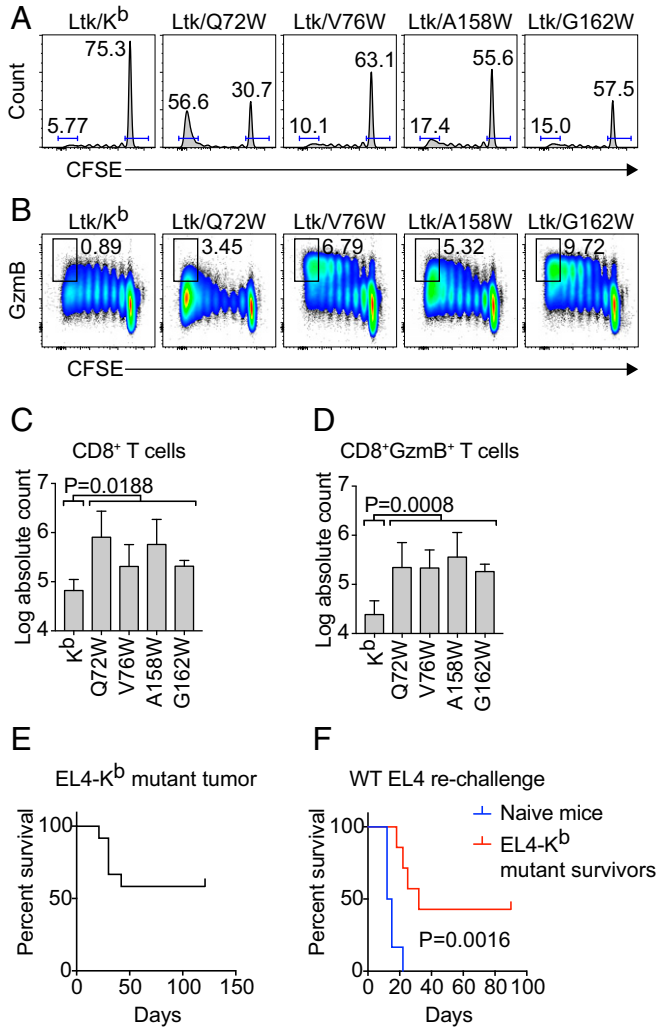

Fig. 4. Recognition of K^b mutants drives CD8 T cell expansion and differentiation in vitro. (*A–D*) CD8 T cells from B6C3F1/J mice were isolated from total splenocytes and labeled with CFSE before coculture with stable L cell transfectants expressing K^b and K^b mutants. Culture media was supplemented with 30 U/mL rhIL-2, 0.5 ng/mL rhIL-7, and 5 μg/mL anti-CD28 mAb. Flow cytometry was used to quantify numbers of cells that were Granzyme B^+ and fully divided. (*A* and *B*) Cells were gated on viable $CD3^+CD8^+$ T cells. (*A*) Histograms show T cell division measured by dilution of CFSE. Gates indicate the frequencies of CD8 T cells fully divided (on the left) and undivided (on the right) in each panel. (*B*) Bivariate plots show expression of Granzyme B over the course of cell division with gates indicating frequencies of CD8 T cells both positive for Granzyme B and fully divided. The absolute counts of (*C*) fully divided CD8 T cells and (*D*) fully divided Granzyme B^+ CD8 T cells are quantified. Bars represent the mean ± SD of $n = 3$ independent experiments. Statistical significance was tested using unpaired, two-tailed *t* tests comparing K^b vs. pooled K^b mutants. (*E* and *F*) Survival analysis of (*E*) EL4-K^b mutant implanted B6 mice ($n = 12$) and (*F*) naïve B6 ($n = 6$) and EL4-K^b mutant survivors ($n = 7$) rechallenged with WT EL4 are shown. Statistical significance was evaluated using the log-rank (Mantel–Cox) test.

T cells in response to stimulation by the L cell transfectants after 5 d in culture as measured by dilution of CFSE and up-regulation of the Granzyme B effector molecule. Compared with stimulation with WT K^b, stimulation with the K^b mutants resulted in an increase in the proportion of CD8 T cells that were fully divided and that had up-regulated Granzyme B (Fig. 4 *A* and *B*). Quantification of total numbers of CD8 T cells responding to K^b mutant stimulation are shown in Fig. 4 *C* and *D*, enumerating the total number of CD8 T cells that fully divided and the total number of fully divided CD8 T cells that had up-regulated Granzyme B, respectively, in response to stimulation with WT K^b and K^b mutants.

Next, we evaluated the ability of the K^b mutant molecules to function as alloantigens in vivo. EL4 lymphoma cells, which uniformly grow unabated in B6 mice, were transfected with K^b mutant genes and cloned by limiting dilution before implantation into B6 mice. Fifty-eight percent of the mice survived tumor challenge (Fig. 4*E*). The survivors and a set of naïve animal controls were challenged in a follow-up study with WT EL4 expressing only native K^b (Fig. 4*F*). Although all of the naïve hosts succumbed to tumor challenge with a median survival of 13.5 d, the survivors of an EL4-K^b mutant transplant resisted reengraftment with WT tumor with a median survival of 32 d and long-term survival of 43% of the mice ($P = 0.0016$). This study demonstrates that expression of predicted K^b mutant MHC molecules in EL4 lymphoma cells can induce tumor rejection and a recall response to WT EL4 rechallenge.

Functional Expression of WT K^b and Mutants Q72W and G162W in Vivo Following Transduction with Adenovirus. To test the functional role of the predicted K^b mutants as antigen-presenting molecules in vivo, we generated replication defective adenovirus vectors based on lower seroprevalence human adenovirus serotype 6 (Ad6) (42, 43) encoding WT K^b or the K^b mutants Q72W and G162W. Intradermal injection of these vectors into BALB/c mice resulted in transduction of professional APC residing within the subcapsular sinus of the right subiliac draining LN (dLN) (44) (*SI Appendix*, Fig. S4). BALB/c hosts exhibited statistically significant expansions of multiple broadly defined immune cell types within the dLN but not nondraining LNs (ndLN) or spleen 4 d postinfection (dpi) (*SI Appendix*, Fig. S5). To assess the in vivo CD8 T cell response to K^b mutants in a setting of tolerance, we transferred CFSE-labeled CD45.1 congenic B6 CD8 T cells to B6 CD8-KO hosts before infecting with Ad vectors by intradermal injection at the base of the tail. Fig. 5 shows the response of transferred CD8 T cells at 4 dpi with the K^b W mutants. Transferred CD8 T cells responded to recognition of K^b mutants Q72W and G162W in vivo with proliferation and up-regulation of the activation marker CD44 (Fig. 5*A*). Recognition of Q72W and G162W in vivo also resulted in effector differentiation of responding CD8 T cells as measured by down-regulation of the LN homing marker CD62L (Fig. 5*B*). Transferred CD8 T cells did not respond to recognition of WT K^b to any greater extent than to control Ad as shown by the lack of both proliferation and effector differentiation (Fig. 5 *A* and *B*). Quantification of total numbers of $CD44^+$ CD8 T cells that were fully divided and total numbers of effector differentiated CD8 T cells that had responded to recognition of K^b mutants in vivo is shown, respectively, in Fig. 5 *C* and *D*. Recognition of K^b mutants Q72W and G162W in vivo resulted in significantly increased total numbers of transferred CD8 T cells that had fully divided (Fig. 5*C*) and had undergone effector differentiation (Fig. 5*D*) compared with total numbers of transferred fully divided CD8 T cells responding to recognition of WT K^b. This indicated that in a setting of tolerance to K^b, recognition of predicted K^b mutants Q72W and G162W in the context of Ad infection was sufficient to activate a K^b mutant alloresponse. Therefore, these molecules must function appropriately as antigen-presenting molecules and possess demonstrable capacity to activate alloreactive T cells from the H-2^b selected repertoire.

K^b Mutants Q72W and G162W Elicit a Potent Cytotoxic T Lymphocyte Response Capable of Killing K^b-Expressing Targets in Vivo. We next queried the ability of K^b mutant activated CD8 T cells to functionally cross-react with WT K^b by testing whether cytotoxic T lymphocytes (CTL) responding to K^b mutant Ad could eliminate WT K^b targets in vivo. Fully allogeneic BALB/c mice were infected

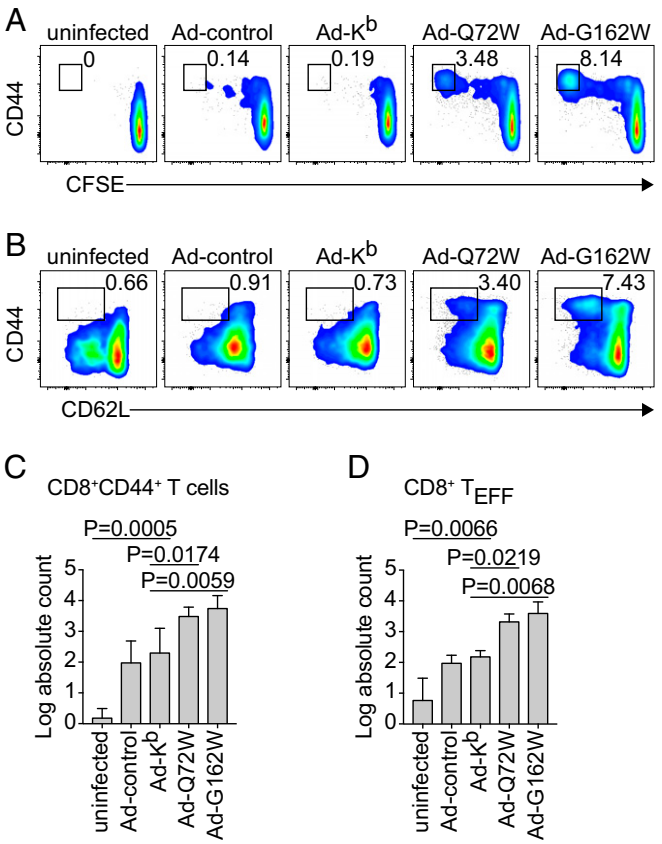

Fig. 5. Infection with Ad vectors encoding K^b mutants drives CD8 T cell expansion and differentiation in vivo. (*A–D*) B6 CD8-KO recipients were transferred with donor CFSE labeled CD45.1 congenic B6 CD8 T cells before being infected with Ad-K^b, Ad-Q72W, or Ad-G162W by intradermal injection. Control mice were uninfected or infected with a control Ad encoding a GFP-Luciferase fusion protein (Ad-control). Cells were processed from the dLN at 4 dpi. Flow cytometry was used to quantify activated transferred CD8 T cells that had undergone cell division as measured by expression of CD44 and dilution of CFSE (*A*) and effector differentiation as measured by expression of CD44 and down-regulation of CD62L (*B*). Absolute counts of $CD44^+$ fully divided (*C*) and $CD44^+CD62L^-$ (*D*) donor CD8 T cells are shown for each of the Ad infections tested. Bars represent means ± SD of $n = 3$ independent experiments. Statistical significance was calculated using repeated measures one-way ANOVA with Dunnett's multiple comparisons test.

with Ad vectors encoding WT K^b or K^b mutants Q72W and G162W by intradermal injection at the base of the tail. Mice were given IV transfers of B6 and BALB/c fluorescently labeled target cells at 4 dpi to assess in vivo killing. Flow cytometry was used to quantify the total number of target cells recovered from the spleen after 4 h (Fig. 6). Infection with Ad-K^b resulted in the nearly complete elimination of allogeneic B6 target cells (Fig. 6*A*, *Middle*, and Fig. 6*B*, *Left*). Syngeneic BALB/c target cells were spared. BALB/c mice infected with Ad-Q72W or Ad-G162W also nearly completely eliminated B6 targets (Fig. 6*A*, *Right*, and Fig. 6*B*, *Left*). These findings indicate that alloreactive CTL responding to the K^b mutants were capable of cross-reacting on WT K^b expressing target cells, an expected outcome if the WT and mutant molecules share the spectrum of presented peptides, and the perturbation of the TCR–pMHC interface does not grossly alter the ability of activated VαVβ TCR combinations expressed by CTL to recognize parental pMHC. Cross-reaction of alloreactive CTL responding to K^b and K^b mutants on C3H third-party target cells was also observed (Fig. 6*A*, third, fourth, and fifth panels, and Fig. 6*B*, *Right*). Quantification of target cell killing is shown in Fig. 6*B* and indicates that percent killing, calculated from total numbers of B6 and C3H targets relative to syngeneic BALB/c targets across each of the infections, is comparable for CTL activated by WT and the K^b mutant molecules.

Alloreactive CTL Responding to K^b Mutant G162W in Vivo Are Cross-Reactive on Self-K^b Expressing Targets, Indicating a Break in Self-Tolerance. Having shown that infection with Ad-K^b, Ad-Q72W, and Ad-G162W resulted in the activation and differentiation of alloreactive CTL that were cross-reactive on K^b in an allogeneic setting, we next wanted to test the hypothesis that recognition of the K^b W mutants in a tolerant setting would result in the activation and differentiation of CTL capable of cross-reacting on self. To test this hypothesis we performed an in vitro killing assay using fluorescently labeled, C3H-derived L cell transfectants stably expressing WT K^b, G162W, or L^d as targets and CD8 T cells isolated from Ad-infected mice as effectors. B6C3F1 mice were infected with Ad-K^b, Ad-G162W, and control Ad by intradermal injection at the base of the tail. CD8 T cells were isolated from the right subiliac dLNs at 4 dpi and used as effectors against the L cell targets to measure the capacity of G162W alloreactive responders to cross-react on syngeneic K^b. Flow cytometry was used to quantify the total numbers of target cells remaining after 8 h in culture with effectors. Fig. 7*A* shows representative plots of target cell recovery. Target cell population

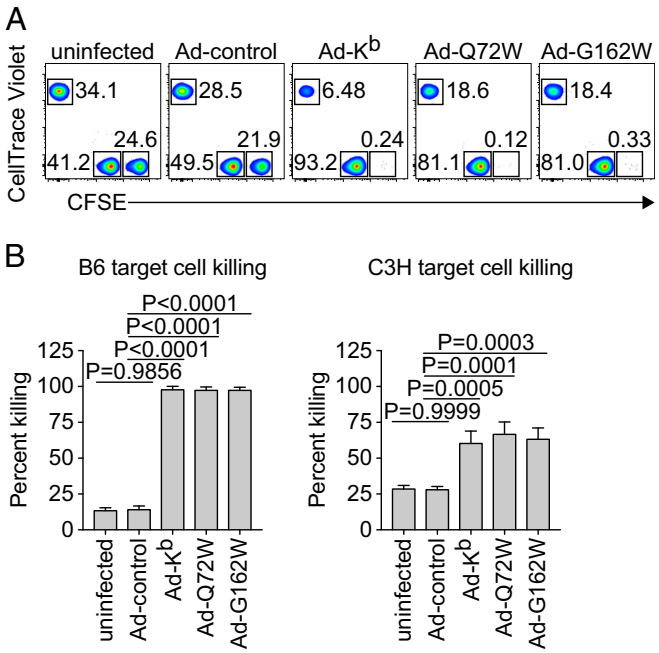

Fig. 6. Ad-K^b mutant infection of BALB/c allogeneic hosts drives potent CTL responses that cross-react on native K^b expressing B6 targets in vivo. (*A* and *B*) BALB/c mice were infected with Ad-K^b, Ad-Q72W, or Ad-G162W by intradermal injection at the base of the tail. An in vivo CTL assay was performed at 4 dpi. Allogeneic B6 and syngeneic BALB/c splenocytes were differentially labeled with high and low concentrations of CFSE. Third-party allogeneic C3H splenocytes were labeled with CellTrace Violet (CTV). Labeled targets were transferred to infected BALB/c hosts by IV injection. After 4 h, labeled target cells were recovered from infected BALB/c host spleens and quantified by flow cytometry. (*A*) Representative plots of target cell recovery are shown for $CFSE^{HI}$ B6 targets, $CFSE^{LO}$ BALB/c targets, and CTV^+ C3H targets. Gate statistics indicate frequency of total target cells recovered. (*B*) Quantification of B6 (*Left*) and C3H (*Right*) target cell percent killing was made relative to BALB/c target percent killing. Bars represent means ± SD of $n = 3$ independent experiments. Statistical significance was tested using one-way ANOVA with Dunnett's multiple comparisons test comparing percent killing from each in vivo CTL to Ad-K^b.

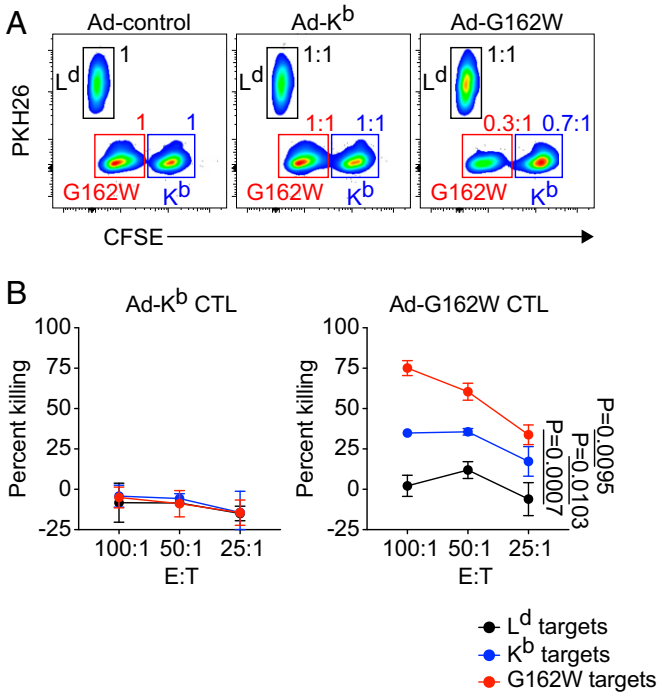

Fig. 7. Ad-K^b mutant infection in a setting of tolerance activates self-reactive CTL capable of killing K^b expressing targets. (*A* and *B*) B6C3F1/J mice were infected with Ad-control, Ad-K^b, and Ad-G162W by intradermal injection at the base of the tail. CD8 T cells were isolated from right subiliac dLN of infected animals at 4 dpi and cultured with fluorescently labeled L cell targets stably expressing K^b, G162W, or L^d in an in vitro killing assay. K^b and G162W targets were labeled with high and low concentrations of CFSE. L^d targets were labeled with PKH26. After 8 h, target cells were harvested and quantified by flow cytometry. (*A*) Representative plots of target cell recovery at effector to target ratio (E:T) 100:1 are shown for Ad-control (*Left*), Ad-K^b (*Middle*), and Ad-G162W (*Right*). Gate statistics for target cells from Ad-K^b (*Middle*) and Ad-G162W (*Right*) infections show ratios compared with the corresponding targets from the Ad-control infection group (*Left*). (*B*) Percent killing of each target cell population for Ad-K^b and Ad-G162W infections is shown relative to percent killing of each target cell population from the Ad-control infection group across each of the three effector to target ratios tested (E:T). Symbols and error bars represent the means ± SD of $n = 3$ independent experiments. Statistical significance was tested using repeated-measures two-way ANOVA with Tukey's multiple comparisons test comparing the K^b, G162W, and L^d target percent killing curves to each other.

gate statistics from Ad-K^b and Ad-G162W effector cultures are shown as ratios comparing against the corresponding target cells from the Ad-control effector culture (Fig. 7*A*).

In this experiment, CTL were primed by endogenous APC expressing self and viral peptides. In the cytotoxicity assay, CTL recognize L cell–derived peptides in the context of expressed MHC class I molecules. Although the L cells may express neo-antigens relative to the parental C3H strain, the primed CTL should recognize only peptides common to both the endogenous APC and the L cell targets. CTL elicited by Ad-K^b and Ad-control failed to eliminate K^b, G162W, and L^d targets, demonstrating that preexisting tolerance for L cell peptides presented in the context of K^b was present in these B6C3F1 hosts (Fig. 7*A*, *Left* and *Middle*, and Fig. 7*B*, *Left*). In contrast, CTL elicited by Ad-G162W infection eliminated ∼70% of G162W targets compared with CTL elicited by Ad-K^b and Ad-control (Fig. 7*A*, *Right*, red gate, and Fig. 7*B*, *Right*, red line). This indicated that recognition of G162W in the context of Ad infection could activate alloreactive CTL capable of potent killing against G162W L cell targets. Strikingly, the alloreactive CTL elicited by Ad-G162W also eliminated ∼30% of syngeneic K^b but not L^d targets, compared with CTL elicited by Ad-K^b and Ad-control viruses, which did not lyse any of the targets (Fig. 7*A*, *Right*, blue gate, and Fig. 7*B*, *Right*, blue line). This indicated that alloreactive CTL responding to recognition of G162W in vivo were capable of significant cross-reaction on L cell targets expressing self-K^b. The cross-reactivity of mutant stimulated CTL on the WT targets is consistent with our hypothesis that the peptides recognized in the context of the mutant G162W are shared by the WT K^b targets. Fig. 7*B* shows the quantification of target cell killing, calculated from total target cell numbers, from Ad-K^b and Ad-G162W induced effectors relative to target cell killing from Ad-control–induced effectors.

Whereas a break in tolerance induced by Ad-G162W infection indicates recognition of undefined self-peptides, we tested the possibility that a break in tolerance might be directed at specific self-peptides. We evaluated this question in RIP-OVA^{HI} mice (45). Previous reports indicate that the RIP-OVA^{HI} animals are deeply tolerant to OVA (46), and our efforts to induce anti-OVA responses in these mice using conventional vaccines have been consistent with that report. The animals were coinfected intradermally with Ad-OVA plus Ad-K^b or Ad-G162W to coexpress OVA antigen and K^b mutant molecules in the same APC. Mice were evaluated for OVA-specific T cell responses 7 dpi using in vivo CTL and in vitro ELISpot assays (Fig. 8). Although RIP-OVA^{HI} mice failed to respond when coinfected with Ad-K^b, significant OVA-specific CTL activity (Fig. 8*A*) and IFNγ secretion (Fig. 8*B*) were observed in Ad-G162W coinfected animals, demonstrating an antigen-specific break in self-tolerance. The ability of immunized RIP-OVA^{HI} mice to lyse OVA-pulsed target cells in vivo is remarkable given that the animal is replete with endogenous cold targets presenting OVA. We previously have not been able to raise any measurable response against the SIINFEKL OVA-derived self-peptide in RIP-OVA^{HI} mice, an experience in line with reports by others (46). We now report our ability to overcome this profound tolerance. Albeit modest in magnitude, the in vivo CTL and in vitro ELISPOT activity indicate responses to OVA vaccination previously unreported in these highly tolerant animals. These findings demonstrate the ability of engineered MHC class I molecules to activate—in an antigen-specific manner—quiescent, self-reactive T cells present in even a highly tolerant immune repertoire. Although the magnitude of the induced autoimmune responses were small in relation to the responses induced using nonself antigens (*SI Appendix*, Fig. S6), our ability to induce them provides an avenue for generating immunity against weak antigens, a goal in cancer immunotherapy.

Thus, in addition to inducing immune responsiveness to a broader, undefined set of self-peptides, we also have induced immune responsiveness to a known self-antigen. These findings are supported with three assays: one targeting self-antigens expressed by fibroblasts (Fig. 7), a second demonstrating the ability of CTL to kill self-peptide pulsed lymphocyte targets expressing self-MHC in vivo (Fig. 8*A*), and a third measuring IFNγ in response to self-peptide expressed on native MHC (Fig. 8*B*).

Finally, we considered the possibility that the introduction of mutant MHC molecules, with the ability of presenting self-peptides in a manner capable of inducing autoreactivity, into APC in lymph nodes might induce systemic autoimmune responses. To evaluate whether in vivo expression of the K^b G162W molecule induces measurable autoimmunity, RIP-OVA^{HI} mice were challenged with Ad-G162W or Ad-K^b and assessed for induced systemic cell death (*SI Appendix*, Fig. S7*A*, *Left*), circulating antinuclear antibodies (*SI Appendix*, Fig. S7*A*, *Right*), and specific depletion of APC from the blood (*SI Appendix*, Fig. S7*B*). No evidence of systemic autoimmunity was detected, indicating that fulminant, generalized autoimmunity does not result from

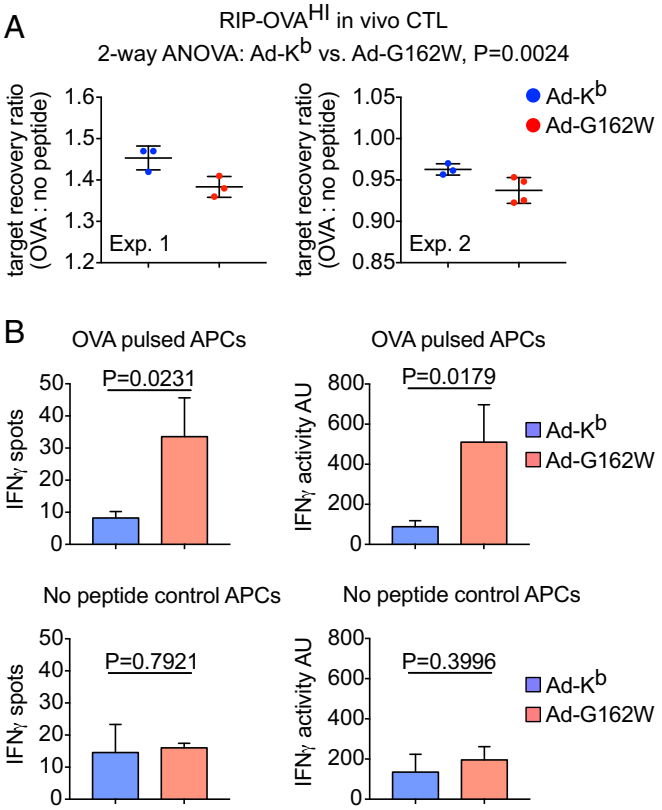

Fig. 8. Coimmunization with Ad-G162W and Ad-OVA in an in vivo model of OVA-specific self-tolerance activates antigen-specific CTL reactive with OVA self-peptide loaded targets. (*A*) An in vivo CTL assay of OVA peptide loaded target cell killing by Ad-OVA/Ad-K^b or G162W coinfected RIP-OVA^{HI} hosts 7 dpi is shown. The absolute counts of recovered OVA peptide loaded B6 target cells were made relative to no peptide control target cells, and the ratios are shown in two separate studies. Experiment 1 (*Left*) shows means ± SD of $n = 3$ independent tests in both Ad-K^b and Ad-G162W groups. Experiment 2 (*Right*) shows means ± SD of $n = 3$ independent tests in Ad-K^b and $n = 4$ independent tests in Ad-G162W groups. Statistically significant OVA peptide loaded target cell killing was evaluated by two-way ANOVA with combined data from both experiments. (*B*) An IFNγ ELISpot assay of CD8 T cells isolated from the spleens of Ad-OVA/Ad-K^b or G162W coinfected RIP-OVA^{HI} hosts 7 dpi is shown. IFNγ spots (*Left*) and activity (*Right*) were quantified in conditions including OVA peptide loaded (*Top*) and no peptide control (*Bottom*) B6 spleen cells that had received 3,300 rad irradiation. Bars represent the means ± SD of $n = 3$ independent tests. Statistical significance was evaluated using *t* tests.

introducing the K^b G162W mutant into the lymph nodes of mice. Furthermore, the mice appeared healthy and groomed throughout all of the experiments described in this report. Therefore, no evidence of systemic autoimmunity was observed. We suspect that immune regulatory mechanisms naturally protecting the body from autoimmune attack limit widespread destruction. To harness targeted autoimmunity, these regulatory mechanisms will need to be subverted.

Discussion

The mature T cell repertoire is biased for self-recognition by positive selection in the thymus for clones expressing self-reactive T cell receptors (47–51). Normally, full activation against self-antigens in the periphery fails due to negative selection against clones expressing receptors with higher affinity for self (9, 12, 52). The residual basal recognition of self-pMHC complexes remaining in the mature repertoire results in subthreshold signaling, an important survival stimulus (13–15). It is possible to activate self-reactive T cells by providing sufficient stimulation, and when the recognized self-ligands are present on target cells at sufficiently high abundance, the induced self-reactive cytotoxic effector T cells can lyse self-target cells (53).

T cells capable of cross-reacting on self-targets have been demonstrated in a number of ways. For example, altered peptide ligands can function as heteroclitic peptide antigens (22). Altered peptide antigens can be generated by targeted amino acid replacement or by using divergent homologs from other species (54–57). Under some circumstances, T cells activated by these antigens have been used effectively to limit tumor growth (58–60). Tumor neoantigens might work in a similar manner. Mutations developing in tumors typically arise during the course of tumor outgrowth and are expected to be present within tumors in a mosaic pattern, except in the infrequent instances where the mutations result in tumor driving events (8, 61). Consequently, if immune responses targeting neoantigens will be effective in controlling tumor growth, tumor cells not expressing the neoantigen also would have to be targeted. This condition would be met when the neoantigen functions as a heteroclitic peptide antigen, inducing T cell reactivity on the native epitope ubiquitously expressed throughout the tumor.

A major challenge for the successful use of altered peptide ligands in the treatment of cancer is the requirement to identify peptides presented at sufficiently high concentrations on the tumor and the engineering of peptide variations that will activate responding T cells for each individual patient. This is a trial and error, candidate approach and therefore not broadly applicable across cancer patients. Although current efforts to identify immunogenic neoantigens for use in personalized cancer vaccines are receiving significant attention (62, 63), a more generalized approach would be valuable.

From studies of alloreactivity we understand that a large fraction of host T cells are capable of responding to foreign MHC molecules, with estimates reaching the 1–10% range of the mature peripheral T cell repertoire (64). However, efforts to introduce a fully allogeneic MHC molecule in tumors for the treatment of melanoma failed even though theoretically, all T cells responding must have exhibited residual affinity for self. For example, the HLA-B27 gene was delivered by intralesion injection as a therapeutic approach for the treatment of melanoma (65), an approach that ultimately failed (66). The inability of alloreactive CTL induced by B27 to control melanoma is likely due to dilution of very few allospecific clones capable of targeting melanoma-associated self-peptides presented by self-MHC of sufficient avidity within the broader distribution of allospecific clones selected by self-peptide-B27 alloantigens from the available repertoire.

The importance of relevant presentation of self-peptide by allogeneic target cells is illustrated by studies of allospecific T cell clones. For example, 2C T cells derived from $H\text{-}2^b$ are strongly activated by the allo-ligands L^d-p2Ca and L^d-QL9 (51, 53, 67–69). Activated 2C are capable of cross-reacting on third-party allo-K^{bm3}-dEV-8 targets, but importantly, activated 2C cannot normally cross-react on self-K^b-dEV-8. It is only when dEV-8 peptide is added at sufficiently high concentrations that activated 2C can cross-react on self-K^b target cells (53). Thus, priming of 2C by the alloantigen L^d is not sufficient for secondary activation by self even though 2C exhibits self-reactivity. What is needed is a way to select for allospecific responders capable of cross-reacting on self-peptides that are presented at sufficient levels.

We reasoned that it might be possible to focus the responding allospecific T cell response on self by stimulating T cells with strong allo-ligands that structurally resemble self. For example, our studies of the K^{dm5} mutant demonstrated that an amino acid substitution outside the peptide-binding groove that presented the same spectrum of self-peptides as the parent molecule could

be recognized by H-2^d allospecific T cells (70). An earlier study showed a similar result with a designed K^b mutant molecule (71, 72). However, in both cases, cross-reaction back on self-target cells was not observed. We speculate this failure might be due to changes in the orientation of TCR on the mutant MHC.

Therefore, we undertook an approach using MM modeling of published TCR-pMHC X-ray crystal structures to discover enhancing mutations that might preserve the normal presentation of self-peptides to TCR. We found four tryptophan mutations predicted by MM to enhance TCR binding at key positions in each of five receptor–peptide–ligand structures that did not appear to alter peptide interactions. All four K^b W mutants were immunogenic to H-2^b–restricted T cells in functional tests, including sensitizing syngeneic hosts against tumor rechallenge. One of the variants, G162W, was found to present high concentrations of the peptide SIY in an enhanced manner to the m67 scTCR. Therefore, G162W exhibited the properties we thought would be required of an alloantigen capable of inducing a focused response that could functionally cross-react on self to break tolerance. We found that G162W introduced by adenoviral infection strongly activated CTL that were capable of killing G162W targets, and importantly could also cross-react on self-K^b, as measured by the killing of K^b expressing targets in vitro and in vivo. This result suggests the G162W mutant was capable of focusing the alloreactive T cell response on self-pMHC complexes present in APC that were shared by the target cells and presented in sufficiently high enough concentration to facilitate the cross-reaction on self.

In addition to revealing interactions between TCR and engineered pMHC molecules that are capable of inducing self-reactive T cell responses, these findings may have translatable implications for the treatment of cancer. We have shown that altered self-MHC mutants can be introduced in tumors promoting alloantigen-driven rejection of primary tumor implants and secondary rejection of native tumor upon rechallenge. In addition, in vivo coinfection with Ad vectors encoding MHC mutant genes and Ad vectors encoding self-antigen focused a self-reactive T cell response against the targeted antigen.

Off-target and on-target toxicities have been observed in therapeutic interventions, such as CART therapy, TREG depletion, and combination checkpoint blockade (73). However, these toxicities are largely manageable through clinical intervention. In contrast, introduction of the mutant MHC molecules had no outward dramatic consequence with respect to systemic autoimmunity as judged by the absence of raised lactate dehydrogenase levels in plasma (systemic cell death), by nuclear autoantibody formation (autoimmune marker), or by deletion of antigen-presenting cells (cells presenting mutant MHC in the lymph nodes). The ability to induce CTL activity to weak antigens in the face of tolerance is an important step toward mobilizing the immune response against cancers. Additional studies are required to harness and sustain these responses for the development of functional therapies and to evaluate the enhancement of these responses for off-target autoimmunity.

Materials and Methods

Structure-Based Prediction. TCR–peptide–MHC binding affinity differences were predicted using an empirical score applied to all-atom structure models generated by molecular mechanics simulations with the Internal Coordinate Mechanics (ICM) program (Molsoft LLC). Details of the calculation method are given in ref. 74. Briefly, the X-ray structure of the wild-type TCR–peptide–MHC complex was first regularized by fixing standard covalent bond lengths and angles, imposing quadratic distance restraints between corresponding atoms in the experimental and model structures, and performing local optimization of the total energy function with the restraint potential. Next, the interface residue was mutated and the mutant structure predicted using the ICM molecular mechanics method (75). This involved biased-probability Monte Carlo sampling of the mutated residue conformation with local energy optimization of neighboring residue conformations after each step. A total of 10^6 Monte Carlo steps were applied to ensure convergence. The same procedure was then used to generate the wild-type and mutated peptide–MHC structures without the TCR bound. Finally, an energy-based score was used to calculate the difference between $\Delta\Delta G$ for the mutation in the ternary complex structure and in the isolated peptide–MHC structure. The final predicted binding affinity difference due to the mutation was calculated as an average value over three independent simulations. TCR–peptide–MHC bound coordinate files used in the modeling were downloaded from the Research Collaboratory for Structural Bioinformatics Protein Data Bank (76). Structures used were 1AO7 (35), 1QSE (36), 2GJ6 (37), 2CKB (31), and 1G6R (31).

Mice. C57BL/6, C57BL/6(CD8-KO), BALB/c, and RIP-OVA^{HI} mice were bred in house as needed. mT/mG(red/green) reporter mice (77) were provided by Michael A. Barry (Department of Internal Medicine, Division of Infectious Diseases, Mayo Clinic, Rochester, MN) and bred in house. C57BL/6(CD45.1) congenics were purchased from Charles River. B6C3F1 and C3H mice were purchased from The Jackson Laboratory. Mice used for experiments were between the ages of 8 and 12 wk. Animal experiments were performed with approval by the Mayo Clinic Institutional Animal Care and Use Committee under the provisions of the Animal Welfare Act, Public Health Service Animal Welfare Policy, and principles of the NIH *Guide for the Care and Use of Laboratory Animals* (78).

Flow Cytometry. Cell lines were stained with purified mAbs produced from hybridoma supernatants. Clones to K^b were B8-24-3 (79), K10.56 (80), Y3 (81), and 5F1-2-14 (82). The D^d α3-specific clone 34-2-12 (83) was used to stain K^b/D^d chimeric molecules. FACS reagents used for staining mouse primary cells isolated ex vivo were Ghost Dye Red 780 (13-0865; Tonbo), CD45.1-PerCP/Cy5.5 (A20, 65-0453; Tonbo), CD3ε-PE (145-2C11, 50-0031; Tonbo), CD3ε-APC (145-2C11, 100311; Biolegend), CD8α-BV421 (53-6.7, 100753; Biolegend), CD8α-BV785 (53-6.7, 100750; Biolegend), CD8α-PerCP/Cy5.5 (53-6.7, 100733; Biolegend), CD44-APC (IM7, 103011; Biolegend), CD44-BV650 (IM7, 103049; Biolegend), CD44-BV785 (IM7, 103041; Biolegend), CD62L-APC (MEL-14, 104411; Biolegend), and Granzyme B-PE (GB11, 561142; BD Biosciences). Fluorescent dyes used for T cell proliferation assays and killing assay target quantification were CFSE (C1157; Invitrogen), CellTrace Violet (C34557; Invitrogen), and PKH26 (PKH26GL-1KT; Sigma). Biotinylated peptides and the m67 scTCR were labeled with streptavidin-PE (405203; Biolegend) and streptavidin-BV421 (405225; Biolegend), respectively. Samples were acquired using an LSR II cell analyzer and FACSDiva version 8.0 (BD Biosciences). FACS data were analyzed in FlowJo version 10.4.2 for macOS (FlowJo, LLC).

Class I Genes. K^b/D^d chimeric genes were made as described previously (51). The D^d α3 domain contains a serologic epitope recognized by mAb 34-2-12 (83) used for tracking expression of introduced K^b mutants in our studies. K^b/D^d chimeric genes were cloned into the pUC 18 mammalian expression plasmid. K^b heavy chain tryptophan mutants were generated by site-directed mutagenesis. Expression was verified by staining with mAb 34-2-12 and K^b α1/α2-specific mAbs.

MHC Transfectants. Mouse L cells were transfected using the calcium phosphate technique described previously (84). Thymidine kinase-negative L cells were cotransfected with DNA encoding MHC genes and the Herpes thymidine kinase gene as described previously (85). Cells were selected in HAT medium and screened for expression of the D^d α3 domain by staining with mAb 34-2-12. Human T2 tap-deficient cells expressing K^b have been described previously (86, 87). T2 were transfected with K^b/D^d chimeric genes and K^b/D^d tryptophan mutant chimeric genes by electroporation. Transfectants were selected with G418 Geneticin.

Ad Vectors. Human E1 and E3 deleted replication defective Ads (RD-Ads) were generated as described previously (43, 88). H-2K^b cDNAs were made from L cell K^b transfectant RNA (SuperScript III First Strand Synthesis; Invitrogen), PCR amplified (Expand High-Fidelity; Roche), and cloned (TOPO TA; Invitrogen). The Q72W and G162W mutations were introduced using site-directed mutagenesis (QuikChange II; Agilent). WT and mutant K^b clones were then subcloned into the pAd6-NdePfl-GL-LZL shuttle plasmid using AgeI and SpeI restriction sites. The expression cassette flanked by Ad6 fiber and E4 sequences was removed using NdeI and BlpI and recombined into E1/E3-deleted pAd6 by red recombination in bacteria as described previously (89). RD-Ad-K^b, RD-Ad-Q72W, and RD-Ad-G162W plasmids were linearized with AsiSI, purified, and transfected into 293 cells. Infectious viral particles were passaged in 293 cells and purified by double CsCl banding as described previously (90). Vector particle (vp) concentration was determined by OD_{260}.

Mice were infected with 1×10^{10} vp of the indicated viruses diluted in PBS by intradermal injection at the base of the tail. Dose was based on vector particle concentration rather than infectious units as recommended (91).

Peptide Binding. Mixed solutions of reference peptide SII[C-biotin]FEKL (38) and unlabeled competitor peptides OVA 257-264 (SIINFEKL), TRP2 180-188 (SVYDFFVWL), and VSV 52-59 (RGYVYQGL) were prepared in serum-free DMEM with 12.5 mM Hepes. Reference peptide concentration was 3 μM in all peptide solutions. Competitor peptide concentrations ranged from 100 μM to 100 pM in 10-fold dilutions. MHC expressing L cell transfectants were incubated in peptide solutions for 1 h on ice. Peptide loaded cells were washed, stained with streptavidin-PE, and fixed with 4% PFA. Cells were analyzed by flow cytometry to determine reference peptide binding. Peptides were synthesized by the Mayo Clinic Proteomics Core.

Single-Chain T Cell Receptor. The 2C variant, m67, soluble single-chain TCR has been described previously (39–41). MHC expressing T2 cells were loaded with either 10 μM OVA peptide (SIINFEKL) or 10 μM SIY peptide (SIYRYYGL) diluted in serum-free IMDM for 2 h at 37 °C, 5%CO_2. Peptide-loaded cells were washed before being pulsed with biotinylated m67 scTCR in cold PBS for 30 min on ice. Cells were washed, stained with streptavidin-BV421, washed, and fixed with 4% PFA. Cells were analyzed by flow cytometry to quantify m67 scTCR binding. Peptides were synthesized by the Mayo Clinic Proteomics Core.

T Cell Activation. CD8 T cells were isolated from the spleens of B6C3F1 mice by magnetic enrichment (CD8a+ T cell isolation kit, 130-104-075; Miltenyi Biotec) and fluorescently labeled with CFSE (Invitrogen C1157). 1×10^6 CFSE-labeled CD8 T cells were added to culture with 2.5×10^5 MHC expressing L cell transfectants in tissue culture-treated six-well plates. L cell transfectants were treated with 5,000 rad of gamma irradiation to inhibit their proliferation before culture. Culture medium was RPMI-1640 (11875-093; Gibco) with added 10% FBS (S11150; Atlanta Biologicals), 100 U/mL Penicillin + 100 μg/mL Streptomycin (15140-122; Gibco), 10 mM Sodium Pyruvate (25-000Cl; Corning), 20 mM L-glutamine (25-005Cl; Corning), 1× MEM nonessential amino acids (25-025Cl; Corning), 12.5 mM Hepes (15630-080; Gibco), and 50 μM 2-mercaptoethanol. Medium was additionally supplemented with 1× Insulin-transferrin-selenium (41400-045; Gibco), 30 U/mL rhIL-2 (200-02; Peprotech), 0.5 ng/mL rhIL-7 (200-07; Peprotech), and 5 μg/mL anti-mouse CD28 mAb (clone 37.5, BE0015-1; Bioxcell). Cultures were incubated at 37 °C with 5% CO_2 for 5 d. Culture medium was replaced on days 2 and 4. Cells were analyzed by flow cytometry to quantify proliferation and activation.

In Vivo CTL Killing. For in vivo CTL assays, 10^7 fluorescently labeled target cells were prepared from donor spleens. Targets were transferred by tail-vein IV injection into Ad-infected hosts at 4 or 7 dpi. After 4 h, spleens from the Ad-infected hosts were harvested and processed to single cells. Cells were counted using a hemocytometer and trypan blue. Cells were stained with a fixable viability dye and fixed in 4% PFA. Cells were analyzed by flow cytometry to quantify the number of fluorescently labeled target cells remaining. The frequency of total live cells of each target cell population was multiplied by the total spleen counts to determine target cell absolute counts. Percent killing was determined by the formula shown below.

$$\%\ \text{killing} = \left(1 - \frac{\text{target absolute count}}{\text{control absolute count}}\right) \times 100.$$

In Vitro CTL Killing. For in vitro CTL assays, 2×10^4 fluorescently labeled L cells expressing K^b, G162W, and L^d were used as targets. Effectors were isolated by CD8 enrichment (CD8a+ T cell isolation kit, 130-104-075; Miltenyi Biotec) from the right subiliac dLN of Ad-infected B6C3F1 mice at 4 dpi. Effectors were added to MHC expressing L cell targets in ratios of 100:1, 50:1, and 25:1. CTL assays were cultured for 8 h at 37 °C, 5%CO_2. L cell targets and effectors were then harvested using trypsin-EDTA (25200-072; Gibco), washed, stained with a fixable viability dye, and fixed with 4% PFA. Cells were analyzed by flow cytometry to quantify the number of target cells remaining. CountBright beads were used to determine target cell absolute counts (C36950; Invitrogen). Percent killing was determined by the formula shown above where the numerator indicates L cell target counts from culture with effectors from Ad-K^b– and Ad-G162W–infected mice and the denominator indicates L cell target counts from culture with effectors from Ad-control–infected mice.

Tumor Challenge. C57BL/6 mice were implanted with 5×10^5 EL4-K^b mutant transfectants by s.c. injection in the right flank. Tumor measurements began 14 d postimplantation. Mice were euthanized when tumors reached endpoint criteria. Survivors were rechallenged by s.c. injection of WT EL4 lymphoma in the left flank.

ELISpot. IFNγ ELISpots were performed as described previously (92).

Statistical Analysis. GraphPad Prism version 7.0 was used for statistical analyses. Data were analyzed using Student's *t* tests, one-way and two-way repeated measures and unpaired ANOVA with Dunnett's and Tukey's multiple comparisons tests, and the extra sum-of-squares F test where indicated in the figure legends.

ACKNOWLEDGMENTS. We acknowledge the excellent technical support provided by Michael P. Bell and Kathleen S. Allen. Ajay A. Madhavan, Josephine M. Ju, Jaspreet S. Kohli, and Jack H. Swanson performed experiments that were important for shaping the direction of the described work. The Mayo Proteomics Core and the Mayo Microscopy and Cell Analysis Core also provided important technical support. This work was supported by NIH Grants R21 A1097337, NIH T32 AI07425, and NIH R01 CA178844. This work was additionally supported by grants from the Fraternal Order of Eagles Cancer Fund (Zumbro Aerie 2228 Eagles Club, Rochester, MN), the Mayo Clinic Center for Biomedical Discovery, Mayo Clinic Ventures, and the Mayo Clinic Graduate School of Biomedical Sciences.

1. Houghton AN (1994) Cancer antigens: Immune recognition of self and altered self. *J Exp Med* 180:1–4.
2. Schietinger A, Philip M, Schreiber H (2008) Specificity in cancer immunotherapy. *Semin Immunol* 20:276–285.
3. Ilyas S, Yang JC (2015) Landscape of tumor antigens in T-cell immunotherapy. *J Immunol* 195:5117–5122.
4. Heemskerk B, Kvistborg P, Schumacher TNM (2013) The cancer antigenome. *EMBO J* 32:194–203.
5. Alexandrov LB, et al.; Australian Pancreatic Cancer Genome Initiative; ICGC Breast Cancer Consortium; ICGC MMML-Seq Consortium; ICGC PedBrain (2013) Signatures of mutational processes in human cancer. *Nature* 500:415–421, and correction (2013) 502:258.
6. Schumacher TN, Schreiber RD (2015) Neoantigens in cancer immunotherapy. *Science* 348:69–74.
7. Wittke S, Baxmann S, Fahlenkamp D, Kiessig ST (2016) Tumor heterogeneity as a rationale for a multi-epitope approach in an autologous renal cell cancer tumor vaccine. *OncoTargets Ther* 9:523–537.
8. Felts SJ, et al. (2015) Widespread non-canonical epigenetic modifications in MMTV-NeuT breast cancer. *Neoplasia* 17:348–357.
9. Kappler JW, Roehm N, Marrack P (1987) T cell tolerance by clonal elimination in the thymus. *Cell* 49:273–280.
10. Klein L, Kyewski B, Allen PM, Hogquist KA (2014) Positive and negative selection of the T cell repertoire: What thymocytes see (and don't see). *Nat Rev Immunol* 14: 377–391.
11. Hogquist KA, Jameson SC (2014) The self-obsession of T cells: How TCR signaling thresholds affect fate 'decisions' and effector function. *Nat Immunol* 15:815–823.
12. von Boehmer H, Teh HS, Kisielow P (1989) The thymus selects the useful, neglects the useless and destroys the harmful. *Immunol Today* 10:57–61.
13. Stefanová I, Dorfman JR, Germain RN (2002) Self-recognition promotes the foreign antigen sensitivity of naive T lymphocytes. *Nature* 420:429–434.
14. Surh CD, Sprent J (2008) Homeostasis of naive and memory T cells. *Immunity* 29: 848–862.
15. Takada K, Jameson SC (2009) Naive T cell homeostasis: From awareness of space to a sense of place. *Nat Rev Immunol* 9:823–832.
16. Aleksic M, et al. (2012) Different affinity windows for virus and cancer-specific T-cell receptors: Implications for therapeutic strategies. *Eur J Immunol* 42:3174–3179.
17. Baitsch L, Fuertes-Marraco SA, Legat A, Meyer C, Speiser DE (2012) The three main stumbling blocks for anticancer T cells. *Trends Immunol* 33:364–372.
18. Schietinger A, Greenberg PD (2014) Tolerance and exhaustion: Defining mechanisms of T cell dysfunction. *Trends Immunol* 35:51–60.
19. Robbins PF, Kawakami Y (1996) Human tumor antigens recognized by T cells. *Curr Opin Immunol* 8:628–636.
20. Hara I, Takechi Y, Houghton AN (1995) Implicating a role for immune recognition of self in tumor rejection: Passive immunization against the brown locus protein. *J Exp Med* 182:1609–1614.
21. Naftzger C, et al. (1996) Immune response to a differentiation antigen induced by altered antigen: A study of tumor rejection and autoimmunity. *Proc Natl Acad Sci USA* 93:14809–14814.
22. Dyall R, et al. (1998) Heteroclitic immunization induces tumor immunity. *J Exp Med* 188:1553–1561.
23. Hoffmann MM, et al. (2015) Co-potentiation of antigen recognition: A mechanism to boost weak T cell responses and provide immunotherapy in vivo. *Sci Adv* 1:e1500415.

24. Matsushita H, et al. (2017) The frequency of neoantigens per somatic mutation rather than overall mutational load or number of predicted neoantigens per se is a prognostic factor in ovarian clear cell carcinoma. *OncoImmunology* 6:e1338996.
25. McGranahan N, Swanton C (2017) Clonal heterogeneity and tumor evolution: Past, present, and the future. *Cell* 168:613–628.
26. Anderson KG, Stromnes IM, Greenberg PD (2017) Obstacles posed by the tumor microenvironment to T cell activity: A case for synergistic therapies. *Cancer Cell* 31: 311–325.
27. Khong HT, Restifo NP (2002) Natural selection of tumor variants in the generation of "tumor escape" phenotypes. *Nat Immunol* 3:999–1005.
28. Rosenberg SA, et al. (1998) Immunologic and therapeutic evaluation of a synthetic peptide vaccine for the treatment of patients with metastatic melanoma. *Nat Med* 4: 321–327.
29. Ribas A, Wolchok JD (2018) Cancer immunotherapy using checkpoint blockade. *Science* 359:1350–1355.
30. Harris DT, Kranz DM (2016) Adoptive T cell therapies: A comparison of T cell receptors and chimeric antigen receptors. *Trends Pharmacol Sci* 37:220–230.
31. Garcia KC, et al. (1998) Structural basis of plasticity in T cell receptor recognition of a self peptide-MHC antigen. *Science* 279:1166–1172.
32. Marrack P, Scott-Browne JP, Dai S, Gapin L, Kappler JW (2008) Evolutionarily conserved amino acids that control TCR-MHC interaction. *Annu Rev Immunol* 26:171–203.
33. Rossjohn J, et al. (2015) T cell antigen receptor recognition of antigen-presenting molecules. *Annu Rev Immunol* 33:169–200.
34. Krissinel E, Henrick K (2007) Inference of macromolecular assemblies from crystalline state. *J Mol Biol* 372:774–797.
35. Garboczi DN, et al. (1996) Structure of the complex between human T-cell receptor, viral peptide and HLA-A2. *Nature* 384:134–141.
36. Ding YH, Baker BM, Garboczi DN, Biddison WE, Wiley DC (1999) Four A6-TCR/peptide/HLA-A2 structures that generate very different T cell signals are nearly identical. *Immunity* 11:45–56.
37. Gagnon SJ, et al. (2006) T cell receptor recognition via cooperative conformational plasticity. *J Mol Biol* 363:228–243.
38. Khilko SN, et al. (1993) Direct detection of major histocompatibility complex class I binding to antigenic peptides using surface plasmon resonance. Peptide immobilization and characterization of binding specificity. *J Biol Chem* 268:15425–15434.
39. Holler PD, Chlewicki LK, Kranz DM (2003) TCRs with high affinity for foreign pMHC show self-reactivity. *Nat Immunol* 4:55–62.
40. Zhang B, et al. (2007) Induced sensitization of tumor stroma leads to eradication of established cancer by T cells. *J Exp Med* 204:49–55.
41. Stone JD, et al. (2014) A novel T cell receptor single-chain signaling complex mediates antigen-specific T cell activity and tumor control. *Cancer Immunol Immunother* 63: 1163–1176.
42. Weaver EA, et al. (2011) Characterization of species C human adenovirus serotype 6 (Ad6). *Virology* 412:19–27.
43. Crosby CM, Barry MA (2017) Transgene expression and host cell responses to replication-defective, single-cycle, and replication-competent adenovirus vectors. *Genes (Basel)* 8:E79.
44. Van den Broeck W, Derore A, Simoens P (2006) Anatomy and nomenclature of murine lymph nodes: Descriptive study and nomenclatory standardization in BALB/cAnNCrl mice. *J Immunol Methods* 312:12–19.
45. Blanas E, Carbone FR, Allison J, Miller JF, Heath WR (1996) Induction of autoimmune diabetes by oral administration of autoantigen. *Science* 274:1707–1709.
46. Steinaa L, Rasmussen PB, Gautam A, Mouritsen S (2008) Breaking B-cell tolerance and CTL tolerance in three OVA-transgenic mouse strains expressing different levels of OVA. *Scand J Immunol* 67:113–120.
47. Zinkernagel RM, Doherty PC (1974) Restriction of in vitro T cell-mediated cytotoxicity in lymphocytic choriomeningitis within a syngeneic or semiallogeneic system. *Nature* 248:701–702.
48. Shearer GM (1974) Cell-mediated cytotoxicity to trinitrophenyl-modified syngeneic lymphocytes. *Eur J Immunol* 4:527–533.
49. Bevan MJ (1977) In a radiation chimaera, host H-2 antigens determine immune responsiveness of donor cytotoxic cells. *Nature* 269:417–418.
50. Nikolić-Zugić J, Bevan MJ (1990) Role of self-peptides in positively selecting the T-cell repertoire. *Nature* 344:65–67.
51. Kuhns ST, Tallquist MD, Johnson AJ, Mendez-Fernandez Y, Pease LR (2000) T cell receptor interactions with class I heavy-chain influence T cell selection. *Proc Natl Acad Sci USA* 97:756–760.
52. Mintz B, Silvers WK (1967) "Intrinsic" immunological tolerance in allophenic mice. *Science* 158:1484–1486.
53. Tallquist MD, Weaver AJ, Pease LR (1998) Degenerate recognition of alloantigenic peptides on a positive-selecting class I molecule. *J Immunol* 160:802–809.
54. Hawkins WG, et al. (2000) Immunization with DNA coding for gp100 results in CD4 T-cell independent antitumor immunity. *Surgery* 128:273–280.
55. Gold JS, et al. (2003) A single heteroclitic epitope determines cancer immunity after xenogeneic DNA immunization against a tumor differentiation antigen. *J Immunol* 170:5188–5194.
56. Cole DK, et al. (2010) Modification of MHC anchor residues generates heteroclitic peptides that alter TCR binding and T-cell recognition. *J Immunol* 185:2600–2610.
57. Capasso C, et al. (2017) A novel *in silico* framework to improve MHC-I epitopes and break the tolerance to melanoma. *OncoImmunology* 6:e1319028.
58. Maslak PG, et al. (2010) Vaccination with synthetic analog peptides derived from WT1 oncoprotein induces T-cell responses in patients with complete remission from acute myeloid leukemia. *Blood* 116:171–179.
59. Maslak PG, et al. (2018) Phase 2 trial of a multivalent WT1 peptide vaccine (galinpepimut-S) in acute myeloid leukemia. *Blood Adv* 2:224–234.
60. Buhrman JD, Slansky JE (2013) Improving T cell responses to modified peptides in tumor vaccines. *Immunol Res* 55:34–47.
61. McGranahan N, et al. (2016) Clonal neoantigens elicit T cell immunoreactivity and sensitivity to immune checkpoint blockade. *Science* 351:1463–1469.
62. Ott PA, et al. (2017) An immunogenic personal neoantigen vaccine for patients with melanoma. *Nature* 547:217–221.
63. Sahin U, et al. (2017) Personalized RNA mutanome vaccines mobilize poly-specific therapeutic immunity against cancer. *Nature* 547:222–226.
64. Sherman LA, Chattopadhyay S (1993) The molecular basis of allorecognition. *Annu Rev Immunol* 11:385–402.
65. Doukas J, Rolland A (2012) Mechanisms of action underlying the immunotherapeutic activity of Allovectin in advanced melanoma. *Cancer Gene Ther* 19:811–817.
66. Williams R (2015) Discontinued in 2013: Oncology drugs. *Expert Opin Investig Drugs* 24:95–110.
67. Sha WC, et al. (1990) Positive selection of transgenic receptor-bearing thymocytes by Kb antigen is altered by Kb mutations that involve peptide binding. *Proc Natl Acad Sci USA* 87:6186–6190.
68. Tallquist MD, Pease LR (1995) Alloreactive 2C T cells recognize a self peptide in the context of the mutant Kbm3 molecule. *J Immunol* 155:2419–2426.
69. Tallquist MD, Yun TJ, Pease LR (1996) A single T cell receptor recognizes structurally distinct MHC/peptide complexes with high specificity. *J Exp Med* 184:1017–1026.
70. Pullen JK, Tallquist MD, Melvold RW, Pease LR (1994) Recognition of a single amino acid change on the surface of a major transplantation antigen is in the context of self peptide. *J Immunol* 152:3445–3452.
71. Grandea AG, 3rd, Bevan MJ (1992) Single-residue changes in class I major histocompatibility complex molecules stimulate responses to self peptides. *Proc Natl Acad Sci USA* 89:2794–2798.
72. Grandea AG, 3rd, Bevan MJ (1993) A conservative mutation in a class I MHC molecule outside the peptide binding groove stimulates responses to self peptides. *J Immunol* 151:3981–3987.
73. Giavridis T, et al. (2018) CAR T cell-induced cytokine release syndrome is mediated by macrophages and abated by IL-1 blockade. *Nat Med* 24:731–738.
74. Bordner AJ, Abagyan RA (2004) Large-scale prediction of protein geometry and stability changes for arbitrary single point mutations. *Proteins* 57:400–413.
75. Abagyan R, Totrov M, Kuznetsov D (1994) ICM—A new method for protein modeling and design: Applications to docking and structure prediction from the distorted native conformation. *J Comput Chem* 15:488–506.
76. Berman HM, et al. (2000) The Protein Data Bank. *Nucleic Acids Res* 28:235–242.
77. Muzumdar MD, Tasic B, Miyamichi K, Li L, Luo L (2007) A global double-fluorescent Cre reporter mouse. *Genesis* 45:593–605.
78. National Research Council (2011) Guide for the Care and Use of Laboratory Animals (National Academies Press, Washington, DC), 8th Ed.
79. Köhler G, Lindahl KF, Heusser C (1981) Characterization of a monoclonal anti-H-2Kb antibody. *The Immune System* (Karger Publishers, Basel), Vol 2, pp 202–208.
80. Hämmerling GJ, Rüsch E, Tada N, Kimura S, Hämmerling U (1982) Localization of allodeterminants on H-2Kb antigens determined with monoclonal antibodies and H-2 mutant mice. *Proc Natl Acad Sci USA* 79:4737–4741.
81. Jones B, Janeway CA, Jr (1981) Cooperative interaction of B lymphocytes with antigen-specific helper T lymphocytes is MHC restricted. *Nature* 292:547–549.
82. Sherman LA, Randolph CP (1981) Monoclonal anti-H-2Kb antibodies detect serological differences between H-2Kb mutants. *Immunogenetics* 12:183–186.
83. Ozato K, Mayer NM, Sachs DH (1982) Monoclonal antibodies to mouse major histocompatibility complex antigens. *Transplantation* 34:113–120.
84. Wigler M, Pellicer A, Silverstein S, Axel R (1978) Biochemical transfer of single-copy eucaryotic genes using total cellular DNA as donor. *Cell* 14:725–731.
85. Pease LR, et al. (1993) Amino acid changes in the peptide binding site have structural consequences at the surface of class I glycoproteins. *J Immunol* 150:3375–3381.
86. Heath WR, Kane KP, Mescher MF, Sherman LA (1991) Alloreactive T cells discriminate among a diverse set of endogenous peptides. *Proc Natl Acad Sci USA* 88:5101–5105.
87. Alexander J, Payne JA, Murray R, Frelinger JA, Cresswell P (1989) Differential transport requirements of HLA and H-2 class I glycoproteins. *Immunogenetics* 29:380–388.
88. Crosby CM, et al. (2017) Replicating single-cycle adenovirus vectors generate amplified influenza vaccine responses. *J Virol* 91:e00720-16.
89. Campos SK, Barry MA (2004) Rapid construction of capsid-modified adenoviral vectors through bacteriophage lambda Red recombination. *Hum Gene Ther* 15:1125–1130.
90. Nguyen TV, Anguiano-Zarate SS, Matchett WE, Barry ME, Barry MA (2018) Retargeted and detargeted adenovirus for gene delivery to the muscle. *Virology* 514:118–123.
91. Nyberg-Hoffman C, Shabram P, Li W, Giroux D, Aguilar-Cordova E (1997) Sensitivity and reproducibility in adenoviral infectious titer determination. *Nat Med* 3:808–811.
92. Pavelko KD, et al. (2013) The epitope integration site for vaccine antigens determines virus control while maintaining efficacy in an engineered cancer vaccine. *Mol Ther* 21: 1087–1095.